Naval Research Laboratory

Washington, DC 20375-5320

NRL/MR/6367--20-10,200

Rapid, Ultra-sensitive Assessment of Elemental and Isotopic Compositions of Materials in Extreme Radiation Environments

Evan Groopman
David Willingham

Materials and Sensors Branch
Material Science & Technology Division

Stuart Jackson

Pulsed Power Physics Branch
Plasma Physics Division

Andrew Gangidine

Contractor

Joseph Schumer

Pulsed Power Physics Branch
Plasma Physics Division

November 24, 2020

REPORT DOCUMENTATION PAGE

Form Approved
OMB No. 0704-0188

1. REPORT DATE *(DD-MM-YYYY)*	**2. REPORT TYPE**	**3. DATES COVERED** *(From - To)*
24-11-2020	NRL Memorandum Report	15 Jun 2020 – 30 Sep 2020

4. TITLE AND SUBTITLE

Rapid, Ultra-sensitive Assessment of Elemental and Isotopic Compositions of Materials in Extreme Radiation Environments

5a. CONTRACT NUMBER

5b. GRANT NUMBER

5c. PROGRAM ELEMENT NUMBER

6. AUTHOR(S)

Evan Groopman, David Willingham, Stuart Jackson, Andrew Gangidine*, and Joseph Schumer

5d. PROJECT NUMBER

5e. TASK NUMBER

5f. WORK UNIT NUMBER
1X31

7. PERFORMING ORGANIZATION NAME(S) AND ADDRESS(ES)

Naval Research Laboratory
4555 Overlook Avenue, SW
Washington, DC 20375-5320

8. PERFORMING ORGANIZATION REPORT NUMBER

NRL/MR/6367--20-10,200

9. SPONSORING / MONITORING AGENCY NAME(S) AND ADDRESS(ES)

Naval Research Laboratory
4555 Overlook Avenue, SW
Washington, DC 20375-5320

10. SPONSOR / MONITOR'S ACRONYM(S)

NRL-NISE

11. SPONSOR / MONITOR'S REPORT NUMBER(S)

12. DISTRIBUTION / AVAILABILITY STATEMENT

DISTRIBUTION STATEMENT A: Approved for public release; distribution is unlimited.

13. SUPPLEMENTARY NOTES

*Contractor

14. ABSTRACT

This report presents research conducted by the U.S. Naval Research Laboratory (NRL) to investigate material properties responsible for extending the lifetimes of nuclear reactor components and enhancing their performance and safety. This report contains experimental and modelling results from two complementary investigations of nuclear fuel cladding materials: Zircaloy-4 and aluminum metal. Aluminum metal was deuteron-irradiated to produce neutron-capture and fission product analogs that could be spatially and depth-resolved using mass spectrometry. The trace actinide abundances (U, Th) in Zircaloy-4 were characterized, as were the predicted isotopic transmutations under reactor-scale neutron fluences. The combination of these irradiation and characterization techniques at NRL could allow for rapid-turnaround interrogations of neutron-capture and fission product analogs in reactor-relevant materials. This work will be followed by irradiation of Zircaloy-4 and analysis of the irradiated Zircaloy-4 and aluminum reaction products described herein. The continuation of these studies would also allow for fine-scale interrogation of heterogeneous power profiles within reactor cores and their effects on component longevity.

15. SUBJECT TERMS

16. SECURITY CLASSIFICATION OF:			**17. LIMITATION OF ABSTRACT**	**18. NUMBER OF PAGES**	**19a. NAME OF RESPONSIBLE PERSON**
a. REPORT	**b. ABSTRACT**	**c. THIS PAGE**			Evan Groopman
Unclassified Unlimited	Unclassified Unlimited	Unclassified Unlimited	Unclassified Unlimited	19	**19b. TELEPHONE NUMBER** *(include area code)* (202) 767-8517

Standard Form 298 (Rev. 8-98)
Prescribed by ANSI Std. Z39.18

This page intentionally left blank.

CONTENTS

FIGURES

TABLES

EXECUTIVE SUMMARY

This report presents research conducted by the U.S. Naval Research Laboratory (NRL) to investigate material properties responsible for extending the lifetimes of nuclear reactor components and enhancing their performance and safety. This report contains experimental and modelling results from two complementary investigations of nuclear fuel cladding materials: Zircaloy-4 and aluminum metal. Aluminum metal was deuteron-irradiated to produce neutron-capture and fission product analogs that could be spatially and depth-resolved using mass spectrometry. The trace actinide abundances (U, Th) in Zircaloy-4 were characterized, as were the predicted isotopic transmutations under reactor-scale neutron fluences. The combination of these irradiation and characterization techniques at NRL could allow for rapid-turnaround interrogations of neutron-capture and fission product analogs in reactor-relevant materials. This work will be followed by irradiation of Zircaloy-4 and analysis of the irradiated Zircaloy-4 and aluminum reaction products described herein. The continuation of these studies would also allow for fine-scale interrogation of heterogeneous power profiles within reactor cores and their effects on component longevity.

This page intentionally left blank.

RAPID, ULTRA-SENSITIVE ASSESSMENT OF ELEMENTAL AND ISOTOPIC COMPOSITIONS OF MATERIALS IN EXTREME RADIATION ENVIRONMENTS

1. INTRODUCTION

The U.S. Naval Research Laboratory (NRL) conducted this research to explore new approaches to rapid irradiation and analysis of nuclear reactor component materials. Our effort aims to leverage NRL's unique nuclear materials analysis capabilities to investigate materials properties responsible for extending the lifetimes and performance of these components. Fuel cladding performance and corrosion under irradiation are important properties affecting the safety of spent and in-use fuel. Globally, new fuel technologies are also being developed and implemented to meet nuclear nonproliferation goals. For example, the Advanced Test Reactor (ATR) operated by the Department of Energy (DoE) at the Idaho National Laboratory (INL) has been mandated by Congress to convert from high- to low-enriched uranium (HEU→LEU) fuel by 2030. This presents new challenges because the LEU fuels (e.g., monolithic UMo foils [1, 2]) do not have the same performance or neutronics characteristics as the current fuel and are not mature technologies at present.

This program aimed to precisely irradiate reactor components to track the migration and sequestration of fission and burnup product analogs using two standout capabilities at NRL. The first is the Hawk and Gamble II pulsed power generators in the Plasma Physics Division, which are capable of deuteron and neutron irradiation to mimic trace radioactive isotope production within light water reactor (LWR) materials. The second is the globally unique Naval Ultra-Trace Isotope Laboratory's Universal Spectrometer (NAUTILUS) instrument in the Materials Science and Technology Division capable of tracking the elemental and isotopic migration within these materials with unprecedented sensitivity [3]. Understanding how materials behave in extreme radiation environments is critically important to improving the longevity of current and future nuclear reactors.

This report describes the experimental and modelling results from NAUTILUS analyses of Zircaloy-4 (Zr:Sn alloy), and Hawk deuteron irradiation of pure aluminum metal. The contents of this technical report provide a strong foundation for continued synthesis of nuclear irradiation and analysis capabilities at NRL.

2. APPROACH

2.1 Technical Approach

We used the globally unique NAUTILUS instrument in NRL's Materials Science and Technology Division to characterize the major and trace element compositions of un-irradiated nuclear cladding materials: Zircaloy-4 and aluminum. We used deuteron beams generated by the Hawk pulsed-power generator in the Plasma Physics Division at NRL [4] to irradiate aluminum, in preparation for measurement on the NAUTILUS (Figure 1). Irradiation of Zircaloy-4 and analysis of irradiated Zircaloy-4 and aluminum will follow the work described in this report. The induced radioactivities and transmuted products serve as analogs to neutron-capture and fission products present in LWR materials. Access to research reactors and the ATR is highly competitive and the sample preparation requirements are stringent. The timeframe for sample preparation, irradiation, cool-off, and NAUTILUS analysis is both

Manuscript approved November 18, 2020.

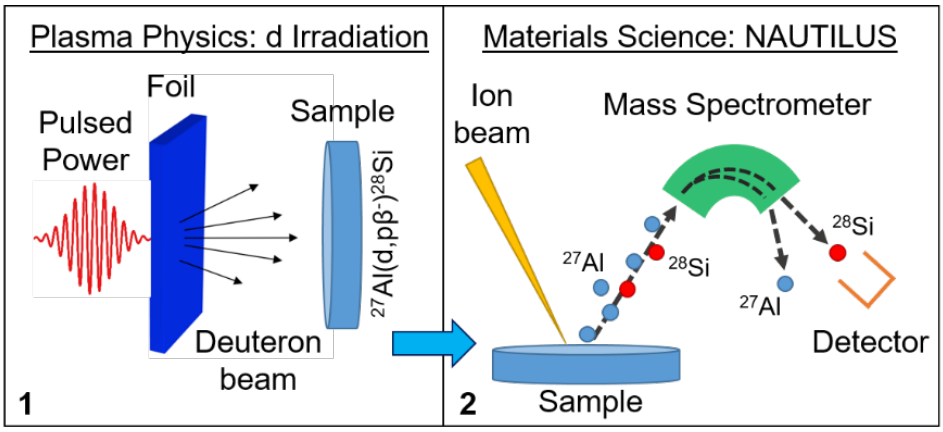

Figure 1: Cartoon schematic of the work effort. (1) Deuteron beam created neutron capture analogs (e.g., ^{27}Al(d,pβ$^-$)^{28}Si) in a sample to be (2) measured by NAUTILUS.

time and cost prohibited. While irradiation in the ATR would be the ultimate goal, a down selection process must first be in place in order to more precisely target the materials, fission products, and radiation environments relevant to LWRs. As part of this down selection process, we used intense deuteron beam interactions in materials to generate measurable analog products to mimic the results from a reactor environment, but with a rapid turnaround time within the scope of this work.

2.1.1 NAUTILUS Analysis of Zircaloy-4 Major & Trace Isotopes

The NAUTILUS instrument in Code 6367 at NRL is a combination secondary ion mass spectrometer (SIMS) and single-stage accelerator mass spectrometer (SSAMS), described fully by Groopman, *et al.* (2020) [3]. The NAUTILUS provides the capability to directly measure trace element and isotope abundances (down to sub-nmol·mol^{-1}). The NAUTILUS removes molecular isobaric interferences that confound conventional SIMS analyses of trace elements. On a conventional SIMS instrument, molecular signals may be present at nearly every mass, even in high-purity samples (see Figure 7 as an example). These molecular signals may overlap trace elements or perturb isotope ratios of interest. The spectrum of molecular interferents is also highly sample-dependent. The NAUTILUS mitigates this drawback of conventional SIMS while retaining the benefits of high lateral and depth resolution, down to micrometer- and 10 nm-scale, respectively. The NAUTILUS may be operated as a conventional small-geometry SIMS instrument with electron multiplier (EM), Faraday cup (FC), and microchannel plate (MCP) detectors, or as a combined SIMS-SSAMS instrument with an EM detector at the SSAMS terminus (for molecule-free measurements). These capabilities are important for discerning the heterogeneous complement of fission and burnup products in irradiated nuclear reactor materials. Recently, the NAUTILUS has been used to investigate other nuclear materials, including tracking fission product migration in nuclear fuel from the Oklo natural nuclear reactors [5], and to the measurement of actinide particles for International Safeguards [6-8].

A coupon of unirradiated Zircaloy-4 was used for this work. Bulk isotope analyses on identical coupons from this Zircaloy-4 ingot measured by inductively coupled plasma mass spectrometry (ICP-MS) contained 0.12 parts-per-million by weight (ppmw) Th and 1.93 ppmw U. These abundances are equivalent to 47 nmol·mol^{-1} (atomic ppb, ppba) Th and 740 ppba U. A 1 cm square sample was cut from the coupon using a diamond saw and inserted into the NAUTILUS with calibration standards, including NIST SRM 610 & 612 trace elements in glass, and U- & Th-rich (%-level) powdered monazite ((Ce,La,Th)PO$_4$). Uranium and thorium abundances were measured on the SSAMS EM relative to Zr abundances measured on the SIMS component of the NAUTILUS. Ethylene gas was used in the SSAMS gas stripping canal to remove molecular isobaric interferences.

Several measurements were performed on the Zircaloy sample to characterize the NAUTILUS' EM detectors and to verify the sample's compositional purity. For quantitative isotope measurements, such as inferring the neutron fluence of irradiated Zircaloy through variations in its Zr isotope abundances, it is critical to characterize the quantum mechanical efficiency and deadtime of each EM and the instrumental mass fractionation. Seven measurements of the $^{91}Zr/^{90}Zr$, $^{92}Zr/^{90}Zr$, $^{94}Zr/^{90}Zr$, and $^{96}Zr/^{90}Zr$ isotopic ratios were made on the SIMS EM under different primary beam intensities to perform this characterization, following the method by Fahey (1998) [9]. These measurements would be reproduced on the SSAMS EM in the future. Measurements of the hydride ratios $^{92}Zr^{1}H/^{92}Zr$ and $^{94}Zr^{1}H/^{94}Zr$ were also made to monitor the ambient hydrogen abundance, which can confound high-precision isotope ratio measurements on conventional SIMS. A mass spectrum (purity) survey was also collected on the SIMS EM by rapidly rastering a 1 nA O^- primary beam over a 25µm×25µm area as the SIMS magnet field was incrementally increased between mass-to-charge ratio (m/z) 5 – 250.

2.1.2 Deuteron Irradiation of Pure Aluminum with Hawk

The Hawk pulsed power generator in Code 6773 at NRL uses a dense plasma focus (DPF) to accelerate deuterons towards a sample at high energies capable of inducing nuclear reactions [10, 11]. A schematic of this process is shown in Figure 2. (1) Neutral deuterium gas is puffed axially from the anode, after which a H^+ and C^+ plasma is injected upstream across the coaxial electrodes. (2) The driver circuit is closed, producing an electromagnetic field, which accelerates the plasma along the electrodes. (3) As the plasma reaches the end of the anode, it is accelerated towards the axis, ionizing and compressing the gas puff. (4) The plasma is compressed in a dense, hot plasma "pinch". High voltage instabilities in the plasma pinch accelerate deuterons towards the sample. Lower energy neutrons are also produced during the DPF, whose energies are diagnostic of the DPF characteristics. For a single "shot", current is driven across the circuit over a period of a few µs. Plasma instabilities that result in deuteron acceleration and sample irradiation last approximately 100 ns during this time. Following sample irradiation, sample radioactivity was measured by an energy-sensitive NaI(Tl) detector to determine the number and type of resulting reactions. The spatial distribution of the induced radioactivity was measured by exposing an X-ray/γ-ray sensitive photographic plate to the sample for five minutes. Neutron energies and emission times were measured using a time-of-flight neutron detector consisting of a fast plastic scintillator and photomultiplier assembly, behind Pb shielding [12].

Using this setup, higher energy neutron beams may also be produced, however they require the use of a conversion foil between the deuteron beam and sample. The deuterons flux is higher than the neutron flux due to losses in the conversion medium. The high-energy deuteron flux is also orders of magnitude larger than the low-energy neutron flux produced in the z-pinch. As a proof-of-concept we decided to use deuterons to induce nuclear reactions instead of neutrons to take advantage of the higher flux, despite neutrons being more directly applicable to a nuclear reactor.

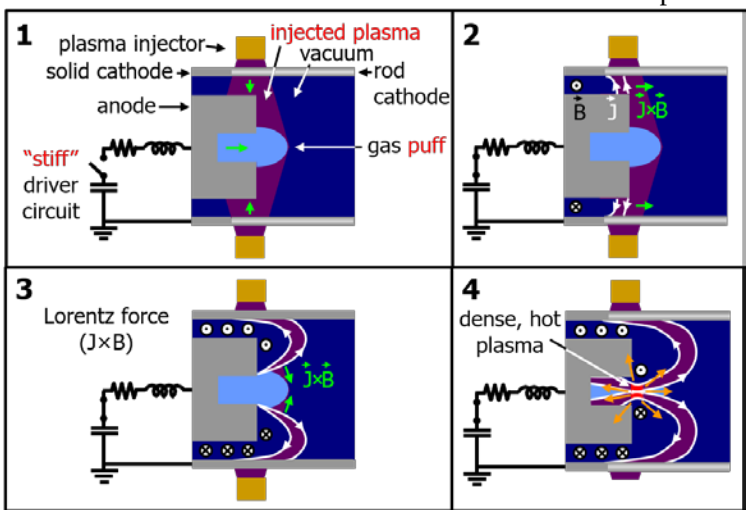

Figure 2: Schematic of the dense plasma focus (DPF) on Hawk that accelerates deuterons to high energies for nuclear reactions.

2.2 Modelling Approach

The experimental work herein was supported by modelling of neutron capture on Zr & Sn isotopes in Zircaloy-4, simulation of the ^{28}Si depth

Table 1 — Nuclear properties of Zr & Sn isotopes and their n-capture products. "--" indicates a stable isotope.

Isotope	Initial Isotope Abundance (%)	Thermal n-capture cross section, σ_0	Resonance Integral, I	$t_{1/2}$
^{90}Zr	51.45	10.66 mb	165.2 mb	--
^{91}Zr	11.22	1.26 b	5.73 b	--
^{92}Zr	17.15	229.2 mb	652.0 mb	--
^{93}Zr	0.00	2.24 b	18.2 b	1.6 Ma
^{94}Zr	17.38	50.69 mb	287.1 mb	--
^{95}Zr	0.00	1.20 b	7.75 b	64 d
^{96}Zr	2.80	20.36 mb	4.23 b	--
^{95}Nb	0.00	7.00 b	58.68 b	35 d
^{95}Mo	0.00	13.6 b	101.8 b	--
^{96}Mo	0.00	447.0 mb	17.52 b	--
^{97}Mo	0.00	2.49 b	16.2 b	--
^{112}Sn	0.97	860.7 mb	30.61 b	--
^{113}Sn	0.00	unknown	unknown	115 d
^{114}Sn	0.66	125.3 mb	6.46 b	--
^{115}Sn	0.34	58.22 b	19.84 b	--
^{116}Sn	14.54	125.1 mb	12.18 b	--
^{117}Sn	7.68	1.08 b	17.94 b	--
^{118}Sn	24.22	215.6 mb	5.28 b	--
^{119}Sn	8.59	2.18 b	5.58 b	--
^{120}Sn	32.58	143.0 mb	1.14 b	--
^{121}Sn	0.00	unknown	unknown	44 y
^{122}Sn	4.63	139.6 mb	954.4 mb	--
^{123}Sn	0.00	unknown	unknown	129 d
^{124}Sn	5.79	137.3 mb	7.86 b	--
^{125}Sb	0.00	5.00 b	55.86 b	2.7 Ma

profile from deuteron irradiation of aluminum by Hawk, and modelling of the dense plasma focus region in Hawk to produce the deuteron beam.

2.2.1 Neutron Capture on Zr & Sn Isotopes

Neutron capture "burnup" patterns of Zr & Sn isotopes in neutron-irradiated Zircaloy-4 were modelled to compare these effects to expected instrument precision. Zirconium typically comprises ~98% by weight of Zircaloy-4, while Sn comprises 1.2 – 1.7 wt. %. Both of these elements are therefore highly abundant relative to the detection limits of the NAUTILUS and would be good targets for investigating neutron capture products. Effective neutron capture cross sections were modelled as $\sigma_c = \sigma_0 + r \cdot I$, where σ_0 is the thermal neutron capture cross section for an isotope, I is the resonance integral, and r is the spectral index (ratio of fast/thermal neutrons). This is a simplistic model, which does not include temperature dependence or Westcott *g*-factors, but is useful for an approximate calculation [13]. Two end-member scenarios were used, with r = 0 (completely thermal neutron spectrum) and r = 0.5. Table 1 shows the nuclear parameters used in the calculations [14], and Figure 3 shows the neutron capture reaction pathways. Isotopes with half-lives shorter than 1 day were omitted from the calculations. In

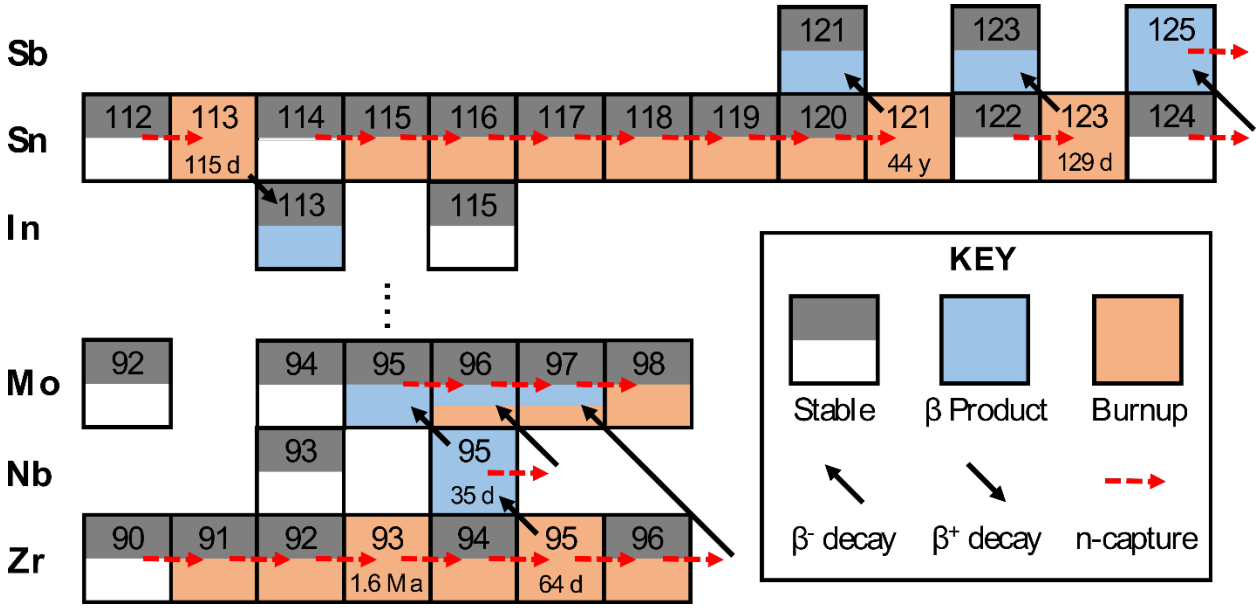

Figure 4: Schematic of neutron capture and beta decay pathways relevant to Zircaloy-4 irradiation. Isotopes with short half-lives omitted. Neutron capture cross sections and decay data given in Table 1.

Figure 5: Deuteron energy spectrum from Hawk and energy-dependent $^{27}Al(D,p\beta^-)^{28}Si$ reaction cross section.Figure 6: Schematic of neutron capture and beta decay pathways relevant to Zircaloy-4 irradiation. Isotopes with short half-lives omitted. Neutron capture cross sections and decay data given in Table 1.

addition, several radioactive Sn isotopes (^{113}Sn, ^{121}Sn, ^{123}Sn) did not have reported neutron capture cross sections, so their abundances and those of their potential n-capture products have some uncertainty. Coupled ordinary differential equations of the form:

$$\frac{dN_{Zr90}(t)}{dt} = -\sigma_{Zr90} \cdot N_{Zr90}(t) \cdot \Phi(t)$$
$$\frac{dN_{Zr91}(t)}{dt} = \sigma_{Zr90} \cdot N_{Zr90}(t) \cdot \Phi(t) - \sigma_{Zr91} \cdot N_{Zr91}(t) \cdot \Phi(t)$$
$$\vdots$$
$$\frac{dN_{Zr95}(t)}{dt} = \sigma_{Zr94} \cdot N_{Zr94}(t) \cdot \Phi(t) - \sigma_{Zr95} \cdot N_{Zr95}(t) \cdot \Phi(t) - \lambda_{Zr95} \cdot N_{Zr95}(t)$$
$$\vdots$$

were solved iteratively for all isotopes in Table 1 over a timespan of 14 months, where N_i is the isotope abundance, and Φ is the neutron flux (assumed homogeneous and constant at 10^{15} $n \cdot s^{-1} \cdot cm^{-2}$, equivalent to the achievable flux at the ATR), and λ_i is the decay constant. Across the ~10 µm scale of individual SIMS & NAUTILUS analyses, a homogeneous neutron flux is a reasonable approximation. A constant flux would not accurately describe the operation of a LWR, however, it is a useful first-order approximation for understanding the potential magnitude of neutron capture effects. The radioactive daughter isotopes in Zircaloy-4 cladding described here all have half-lives considerably greater than short-term shutdown periods, so their relatively abundance during lower-flux periods would not drastically change from β-decay.

2.2.2 Hawk generated $^{27}Al(d,p\beta^-)^{28}Si$ Depth Profile

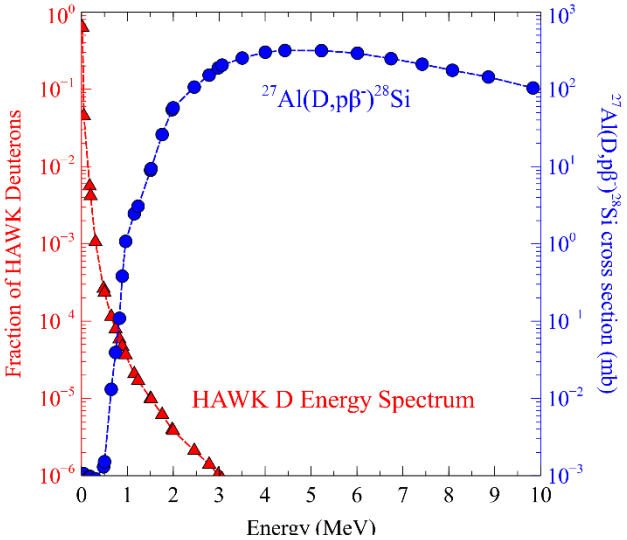

Figure 7: Deuteron energy spectrum from Hawk and energy-dependent ^{27}Al(D,pβ$^-$)^{28}Si reaction cross section.

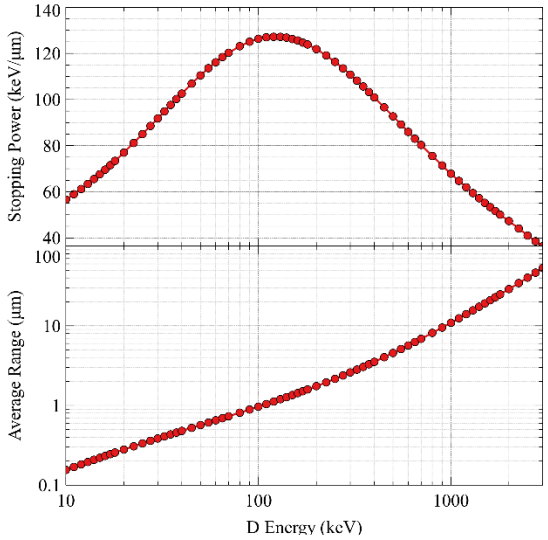

Figure 10: Stopping power and average range of deuterons into aluminum metal calculated using SRIM.

The expected abundance depth profile of the ^{27}Al(d,pβ$^-$)^{28}Si reaction was modelled prior to deuteron irradiation and future NAUTILUS analysis in order to verify the required shot parameters and configuration of Hawk. This modelling was carried out using two Monte Carlo simulations. First, the freely available Stopping Range of Ions in Matter (SRIM) [15] program was used to simulate the electronic and nuclear braking of energetic deuterons being implanted in an aluminum substrate. Simulations for mono-energetic 2-3 MeV Ds, and Ds with an energy distribution matching that of Hawk (Figure 4) were performed. SRIM does not calculate nuclear effects such as neutron or deuteron capture, so the resulting D energy and depth distributions were used as inputs to a subsequent Monte Carlo calculation. Beam damage calculations were not performed as part of these simulations.

Figure 5 (top panel) shows the theoretical stopping power (keV/μm) of aluminum metal on energetic D calculated using SRIM. The average range of a D with initial energy, E, is calculated by integrating the inverse of the stopping power up E (bottom panel). The theoretical calculations and Monte Carlo simulations are well matched, and agree with experimental literature values. For the second Monte Carlo simulation, Ds with energies randomly drawn from the Hawk energy distribution were transmitted through aluminum, using the braking power and earlier simulations to model energy loss. At each step, a randomly generated capture probability was compared to the ^{27}Al(D,pβ$^-$)^{28}Si reaction cross section to determine if a reaction occurred. Capture depths and energies were recorded. Deuterons with less than 500 keV energy were discarded due to their very low and uncertain capture probability.

3. EXPERIMENTS

3.1 Experiment A: NAUTILUS Analysis of Zircaloy-4, Al Major & Trace Isotopes

At the start of the performance period, newer and faster EM detector electronics were built and installed on the SIMS EM to match those on the SSAMS EM of the NAUTILUS, following the description in Groopman, *et al.* (2020) [3]. As is typical with using new EM detectors and electronics, the pulse height distribution of ion was measured to set the proper discriminator threshold, and the system deadtime was evaluated. Figure 6 shows the results of seven measurements (R1-7) of Zr isotope ratios in the Zircaloy-4 at different primary beam intensities. The values are displayed as deviations in parts-per-thousand (‰) from the terrestrial isotope ratio (Table 1) using the formula:

Table 4 — Electron Multiplier deadtime and mass fractionation calibration table. Data and regression lines shown in Figure 6. The regression slope corresponds to the mass fractionation in ‰/amu. The intercept at the reference mass (^{90}Zr) corresponds to the electron multiplier detector deadtime (ns).

Measurement	Slope (‰/amu)	σ	Intercept	σ	^{90}Zr (intercept)	σ	^{90}Zr (mean cps)	Deadtime τ (ns)	σ
1	-14.44	0.54	1326.9	51.0	29.05	2.05	2.98×10^6	9.7	0.7
2	-13.36	0.26	1223.5	24.6	22.64	0.99	2.32×10^6	9.8	0.4
3	-13.88	0.02	1258.1	2.1	10.43	0.08	9.77×10^5	10.7	0.1
4	-13.84	0.23	1254.0	21.2	9.99	0.85	6.34×10^5	15.7	1.3
5	-14.42	0.08	1303.8	7.7	7.68	0.31	6.04×10^5	12.7	0.5
6	-14.70	0.12	1338.3	11.5	16.95	0.46	1.66×10^6	10.2	0.3
7	-13.68	0.09	1234.3	8.9	4.10	0.36	3.24×10^5	12.7	1.1
Weighted Mean	**-13.9**	**0.02**						**10.7**	**0.1**

$$\delta\,{}^{i}\mathrm{Zr}/{}^{90}\mathrm{Zr} \;=\; 1000 \times \left(\frac{{}^{i}\mathrm{Zr}/{}^{90}\mathrm{Zr\_measured}}{{}^{i}\mathrm{Zr}/{}^{90}\mathrm{Zr\_terrestrial}} - 1\right).$$

The slopes of the linear regressions to R1-7 correspond to the instrumental mass fractionation, which includes fractionation during ion extraction, passage through the mass spectrometer, and efficiency at the detector (which is velocity- and ageing-dependent). The intercepts at mass 90 correspond to the detector deadtime, whose effect becomes more pronounced at higher count rates:

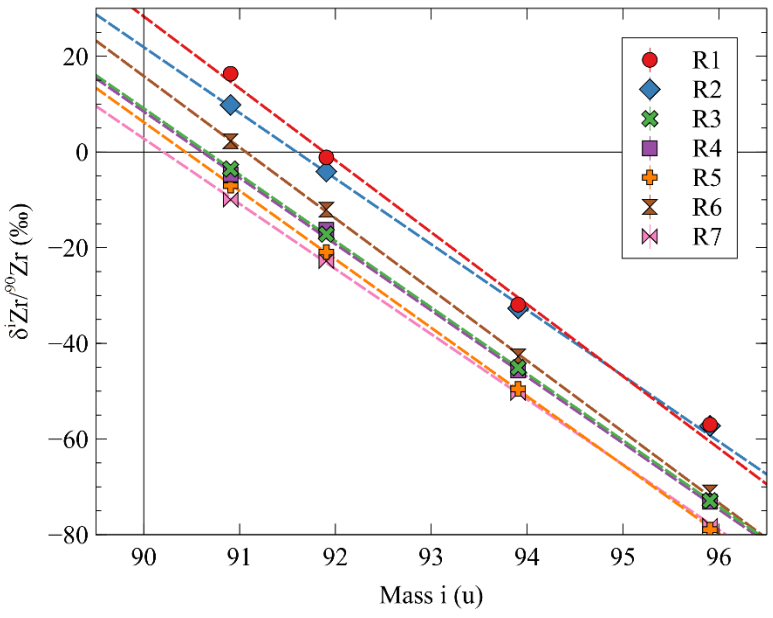

Figure 12: Raw measurements of $\delta^{i}\mathrm{Zr}/^{90}\mathrm{Zr}$ in Zircaloy-4 at varying ion intensities with linear least-squares regression lines (dashed). Slopes of the regressions correspond to the instrumental mass fractionation, and the intercepts of the regressions correspond to the electron multiplier detector deadtime (see Table 1).

$$\mathrm{C_{Measured}} = \frac{\mathrm{C_{True}}}{1 + \mathrm{C_{True}} \cdot \tau} \approx \mathrm{C_{True}} \times (1 - \mathrm{C_{True}} \cdot \tau)$$

where τ is the deadtime in seconds and C is the count rate (counts·s^{-1}) for an individual ion species [6]. Typically, dead time effects become noticeable above 10^5 counts·s^{-1}. With an ideal (non-physical) deadtime of 0 ns or a low count rate, the mass 90 intercepts in Figure 6 would be 0‰. Table 2 shows the results of the measurements in Figure 6. The weighted mean deadtime is 10.7 ± 0.1 ns, with a standard deviation of 2 ns across the measurements. Due to the electronics design, the EM deadtime measured here is 2-5× smaller than those on state-of-the-art commercial SIMS instruments, e.g., [6, 16, 17]. The weighted mean mass

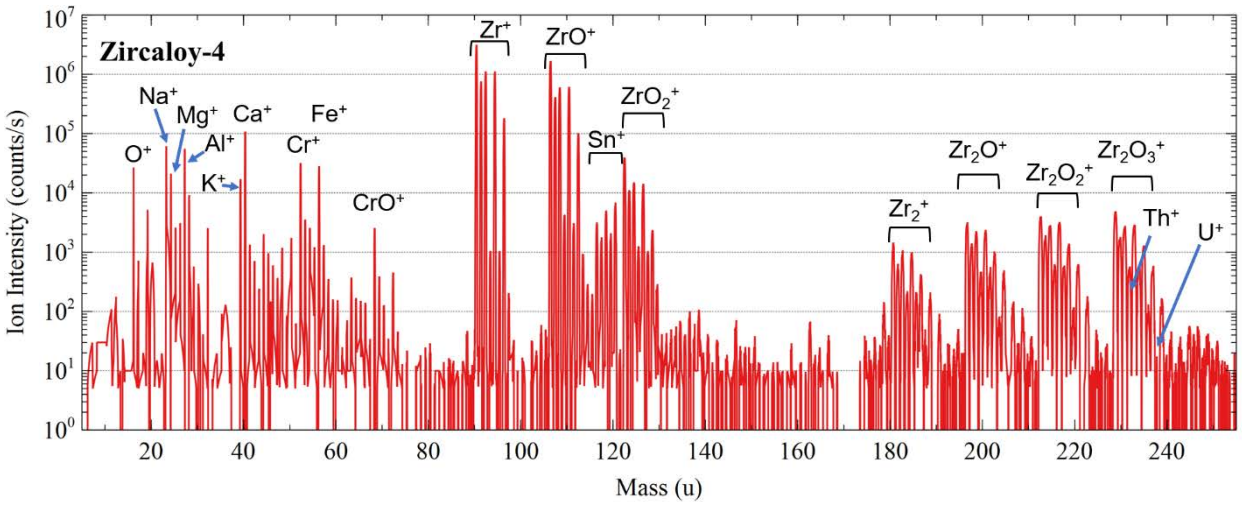

Figure 13: Mass spectrum of Zircaloy-4 on the SIMS EM. Shows atomic and molecular secondary ions from bombardment with O. On the SIMS, Th^+ is obscured by $Zr_2O_3^+$ molecules, and $^{122,124}Sn^+$ are obscured by ZrO_2^+.

fractionation is -13.9 ± 0.02 ‰/amu, with a standard deviation of 0.4 ‰/amu. These measurements indicate that reliable corrections can be made from instrumental artifacts, and ‰-level variations in Zr isotope ratios due to neutron capture are measurable. Tin isotope effects would also be measurable, though would require a more intense primary beam to achieve comparable precision due to their 100× lower abundances.

Figure 7 shows a mass spectrum of the Zircaloy-4 sample using a 1 nA O^- primary ion probe collected on the SIMS EM. The Zircaloy exhibits high purity, as expected, with peaks at Zr, Sn, Cr, Fe, and the oxides of these elements (from bombardment with O^-). The higher mass Sn isotopes (e.g., ^{122}Sn, ^{124}Sn) overlap with intense molecular ZnO_2 peaks. These would be easily deconvolved using the full NAUTILUS, however. Common trace impurities such as Al and Mg are also visible. Sodium, potassium, and calcium peaks are visible as they are common mobile surface contaminants left over from sample washing and they ionize easily; they are not intrinsic to the alloy. Small peaks due to molecular ions and/or trace elements are visible at nearly every m/z, which is common in SIMS. Isotope ratio measurements with the full NAUTILUS instrument would be required to identify and quantify these peaks. SIMS mass spectra are qualitative, in any case, since the yield of each atomic and molecular ion depends upon the local matrix composition, among other effects. Quantification requires homogeneous matrix-matched standards from which relative sensitivity factors (RSFs) for each ion can be calculated.

Thorium and uranium abundances in the Zircaloy-4 were also measured by counting ^{91}Zr and ^{96}Zr on the SIMS FC and EM detectors, and ^{232}Th and ^{238}U on the SSAMS EM. The actinide signals were easily measurable, yielding ~100 counts·s^{-1} from a 1 nA O^- primary beam. Detection limits down to ppba or 100 ppta are achievable. These can be used to infer the destruction of natural "impurity" ^{232}Th and ^{238}U in the Zircaloy via neutron capture and fission, which has been shown to impact the growth of ZrO on fuel cladding [18].

Pure aluminum metal was measured prior to D or n irradiation. Much like the Zircaloy-4 in Figure 7, the mass spectrum showed Al, its oxide ions, and a few surface contaminants, but was otherwise uninteresting and is not reproduced here.

3.2 Experiment B: Deuteron Irradiation of Pure Aluminum with Hawk

Figure 8 shows the γ-ray spectra measured from the Al target before and after a single irradiation shot. Each spectrum was acquired for 5 minutes. The blue curve shows the detector and sample chamber background prior to irradiation. The red and green curves show the γ-ray spectra 5- and 17-minutes post-

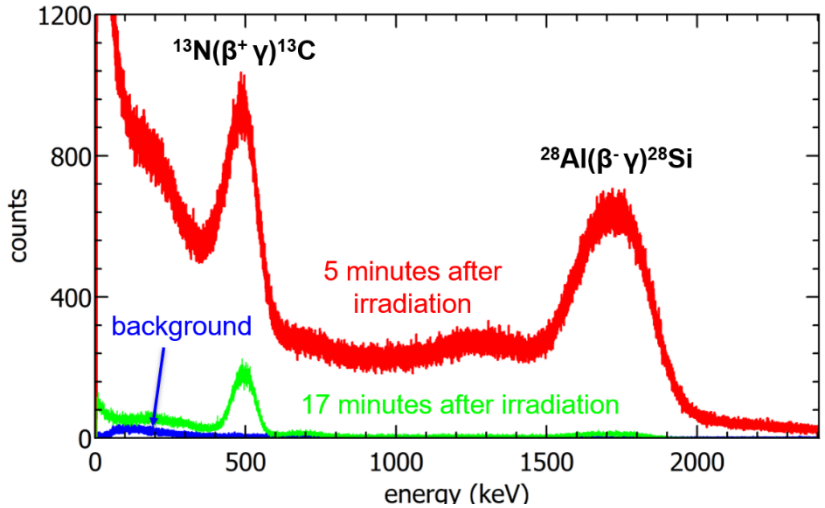

Figure 14: (Red) γ-ray spectrum collected on a NaI detector for 5 minutes, started 5 minutes after deuteron irradiation of aluminum metal. (Green) 5-minute spectrum acquired 17 minutes after irradiation. (Blue) 5-minute background spectrum. The peak at 1779 keV corresponds to γ-ray emission from ^{28}Al(β$^-$ γ)^{28}Si (Q = +5.5 MeV, $t_{1/2}$ = 2.24 m) accompanying the ^{27}Al(d,p)^{28}Al reaction. The peak at 511 keV corresponds to emission from the ^{12}C(d,n)^{13}N reaction (Q = -0.28 MeV, $t_{1/2}$ = 9.96 m). Note: C is injected as part of the plasma.

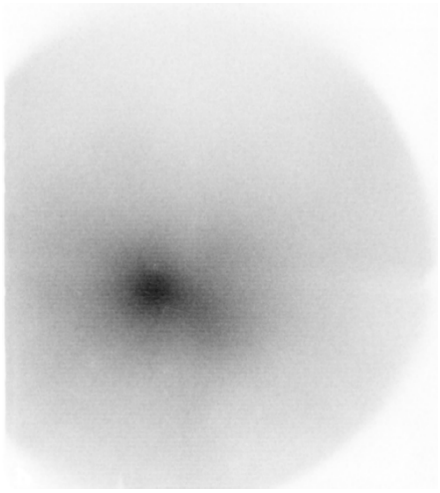

Figure 15: Spatial distribution of induced radioactivity in Al target (11 cm diameter).

irradiation, respectively. The spectra show two prominent peaks at 511 keV and 1779 keV, corresponding to the deuteron activation of ^{12}C and ^{27}Al, and their subsequent decays, respectively. Carbon is present in the DPF plasma and in the sample chamber background. The ^{27}Al(d,p)^{28}Al(β$^-$ γ)^{28}Si reaction has Q = +5.5 MeV and a half-life of $t_{1/2}$ = 2.24 minutes. The ^{12}C(d,p)^{13}N(β$^+$ γ)^{13}C reaction has Q = -0.28 MeV and $t_{1/2}$ = 9.96 minutes. From the integrated peak areas over several half-lives, the magnitude of the reaction products can be estimated. Figure 9 shows the spatial distribution of the deuteron-induced radioactivities across the 11 cm diameter Al target. The highest activity is located at the center of the target (dark contrast), axially aligned with the anode and z-pinch DPF. The NAUTILUS would be used to measure the depth profiles of the produced ^{28}Si in order to characterize the radial energy and flux distributions.

4. MODELING

4.1.1 Neutron Capture on Zr & Sn Isotopes in Zircaloy-4

Figure 10 shows the results of neutron capture calculations for Zr isotopes in Zircaloy-4 as described in Section 2.2.1. Panels A & C show the evolution over time of the Zr delta values and ratios for a purely thermal neutron spectrum. Panels B & D show this evolution where the spectral index r = 0.5. For both scenarios, the changes in the intrinsic Zr isotope ratios and the ingrowths of ^{93}Zr, ^{95}[Zr,Nb,Mo], and ^{97}Mo would be easily measurable given the precision and correction factors presented in Section 3.1. The use of multiple isotope ratios would allow for the deconvolution of neutron fluence, spectral hardness, and/or irradiation time from the Zircaloy. In particular, the hardness of the neutron spectrum has the most pronounced effect on the ^{96}Zr/^{90}Zr and ^{97}Mo/^{90}Zr isotope ratios, as would be expected based upon the nuclear parameters for ^{96}Zr in Table 1 (σ_0 = 20 mb, I = 4 b). The abundances of ^{93}Zr and ^{95}[Zr,Nb,Mo] provide sensitive barometers of lower-fluence irradiations (e.g., under 2 months in the examples). SIMS and the NAUTILUS typically a measurement dynamic range of ~10^7 if using only EM detectors or ~10^{10} if using a combination of EMs and FCs. Therefore, with appropriate standards, all isotope ratios and delta values shown in Figure 10 would be easily measurable.

Figure 11 shows the neutron capture calculation results from Sn isotopes in Zircaloy-4. Tin-119 exhibits relatively strong neutron capture effects and comprises >8% of the intrinsic Sn, making it a good

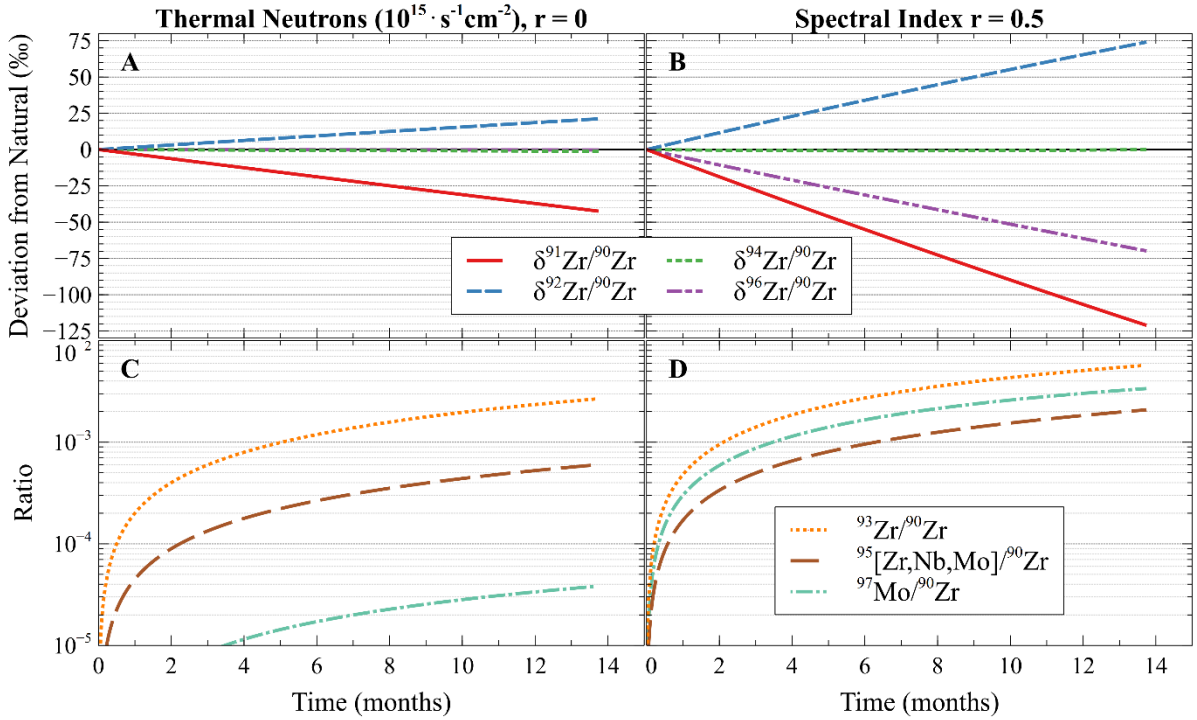

Figure 16: Zirconium isotope delta values and ratios from neutron-capture in Zircaloy-4 under a flux of 10^{15} n·s^{-1}·cm^{-2}. Panels A & C show a purely thermal neutron spectrum, and B & D show the results from a spectral index of 0.5. Measuring multiple isotopic systems would allow for the inference of neutron fluence, spectral harness, and/or irradiation time.

candidate to measure in either a soft or hard spectrum. Tin-118's capture cross section is sensitive to the spectral hardness, with σ_0 = 215 mb and I = 2 b. This can induce the $\delta^{119}Sn/^{120}Sn$ values to range from largely negative to largely positive as the spectral hardness increases, making it a sensitive diagnostic tool. Tin-112 and tin-115 are sensitive to neutron capture at all spectral indices, though their initial abundances are low, 0.97% and 0.34%, respectively. The ingrowths of several radioactive Sn isotopes and their daughters also produce easily measurable isotope ratios. Most Sn isotopes exhibit relatively high sensitivity to fast neutrons. Given the large number of isotopes, the myriad of neutron capture effects would allow for precise determination of neutron fluence and hardness conditions. The sensitivity of the Zr and Sn systems to spectral properties and the large number of measurable isotopes makes them good candidates for examining the heterogeneity of fluxes using samples from different reactor locations.

The isotopes of minor elements in Zircaloy-4, Cr and Fe, would also provide complementary information to Zr and Sn. While not detailed in Table 1, the thermal cross sections of Cr and Fe isotopes are typically a few barns, with I ≈ $\sigma_0/2$ for each isotope [14]. These isotopes exhibit extremely large n-capture effects relative to Zr and Sn, so despite their low initial abundances, so the neutron fluence would be straightforward to estimate (Figure 12). The production of ^{51}V could also be diagnostic for these purposes. As can be seen in Figure 7, Cr^+ and Fe^+ are easily measurable even at 1 nA O^- primary probe intensity on the conventional SIMS. The background abundances of V, Mn, Ni, and Co isotopes are also low due to the high purity of the Zircaloy-4. Chromium and iron are much less sensitive to neutron energy than Zr and Sn, since typically I < σ_0, however, they provide easily accessible and complementary information. Samples irradiated in a test facility such as the ATR will have experienced relatively well known flux profiles.

4.1.2 Hawk generated $^{27}Al(d,p\beta^-)^{28}Si$ Depth Profile

Figure 13 shows the results of the Monte Carlo simulation of $^{27}Al(d,p\beta^-)^{28}Si$ reactions from Hawk irradiation of pure Al metal. The left panel shows the average expected range for the deuterons randomly sampled from the Hawk energy distribution in Figure 4. However, due to electrical and nuclear braking

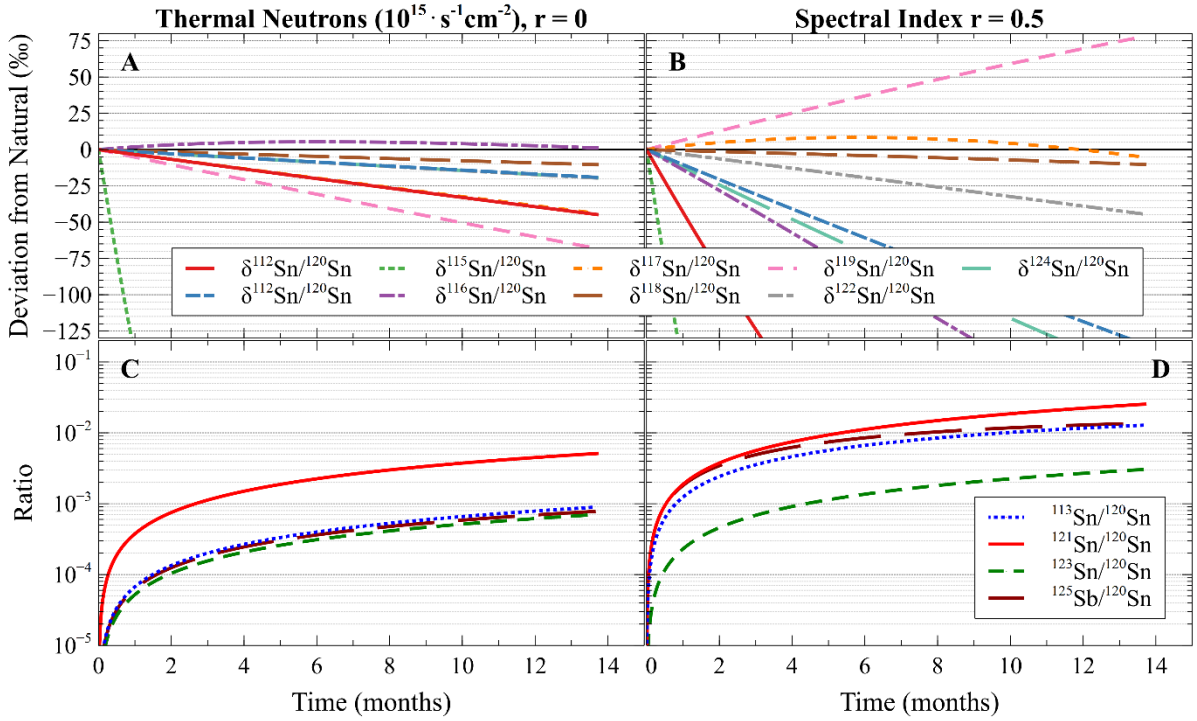

Figure 17: Tin isotope delta values and ratios from neutron-capture in Zircaloy-4 under a flux of 10^{15} n·s^{-1}·cm^{-2}, as in Figure 10. Panels A & C show a purely thermal neutron spectrum, and B & D show the results from a spectral index of 0.5. Tin isotopes are numerous and exhibit a wide range of measurable isotope ratio effects from neutron exposure.

within the aluminum matrix, the deuteron energy rapidly decreases, as does the $^{27}Al(d,p\beta^-)^{28}Si$ cross section. The middle panel shows the distribution of deuteron energies at the time of capture on ^{27}Al. This distribution makes qualitative sense given the monotonically decreasing probability of producing highly energetic deuterons from Hawk combined with the smaller reaction cross sections at lower energies for $^{27}Al(d,p\beta^-)^{28}Si$. The right panel shows the expected depth profile of produced 28Si, which is concentrated within the top several μm of the sample surface. Deuterons that are not captured by ^{27}Al will be implanted, on average, much deeper than the reaction product ^{28}Si.

5. CONCLUSIONS

Based upon the above data, the synthesis of nuclear irradiation and analysis capabilities at NRL may provide a means for rapid turnaround interrogations of reactor-relevant materials. This work demonstrated the NAUTILUS's capabilities to measure trace actinide abundances in unirradiated fuel cladding materials, including Zircaloy-4. The presence of these impurities and their behavior under irradiation may impact the corrosion properties of Zircaloy-4 [18]. The NAUTILUS's capabilities to perform ultra-sensitive actinide detection with lateral and depth resolution down to 10s of micrometers and nanometers, respectively, allows for the 3D reconstruction of abundance heterogeneity. This capability similarly can be used to basic science research objectives, such as the shape and beam characteristics of deuteron and neutron ion beams produced in pulsed power generators, including Hawk. The combination of neutron capture modelling and measurement of Zr isotopes demonstrated that Zr, Sn, Fe, and Cr isotopes could be used to interrogate the neutron fluence and spectral hardness experienced by cladding materials. This information would complement the quantification of trace actinides and their depletion by neutron capture and fission. These studies would also allow for fine-scale interrogation of the heterogeneous power profile within the reactor core, which would be useful to incorporate into reactor modelling codes. The

tools and methods demonstrated here are also applicable to the detection and tracking of mobilized reaction products in reactor fuel and cladding.

This work demonstrated the capability at NRL to irradiate relevant reactor cladding materials for rapid-turnaround characterization of reaction products. The Hawk pulsed power generator was used to produce quantifiable nuclear reaction products within aluminum metal. The combination of nuclear and photo-sensitive detectors on Hawk complement the capability of the NAUTILUS to depth-resolve reaction product concentrations. Future work would include the performing depth-resolved analysis using the NAUTILUS of deuteron-irradiated aluminum produced during this performance period. Modelling of the $^{27}Al(d,p\beta^{-})^{28}Si$ depth profile has shown that reactions produced using the Hawk instrument should be resolvable using the NAUTILUS. This analysis will provide feedback for the down selection process of irradiation parameters used by Hawk and/or more intense pulsed power generators in NRL's Plasma Physics Division, including Gamble II and Mercury. Future work would also include irradiation of Zircaloy-4 at NRL and subsequent analysis. Further development of neutron irradiation schemes using the pulsed power generators would provide the capability for rapid-turnaround irradiations that more closely mimic some properties of a reactor environment. The work demonstrated in this report provides a baseline to develop irradiation and analysis methods for more complicated reactor materials, such as monolithic UMo fuel foils, which are clad with aluminum and a thin diffusion barrier interlayer of zirconium. Correlated and spatially resolved SIMS and X-ray spectroscopy have been performed recently on unirradiated UMo foils, which identified heterogeneities in the chemical and isotopic composition of the fuel meat [2]. Post-irradiation analyses by conventional SIMS would be complicated by the presence of neutron capture and fission products and their molecular ions, making it difficult to deconvolve overlapping signals. The NAUTILUS' capability to remove molecular isobaric interferences on the micrometer-scale would help resolve elemental migration patterns in these samples, especially near fuel, diffusion barrier, and cladding interfaces. Understanding these migration patterns would help increase component longevity and safety.

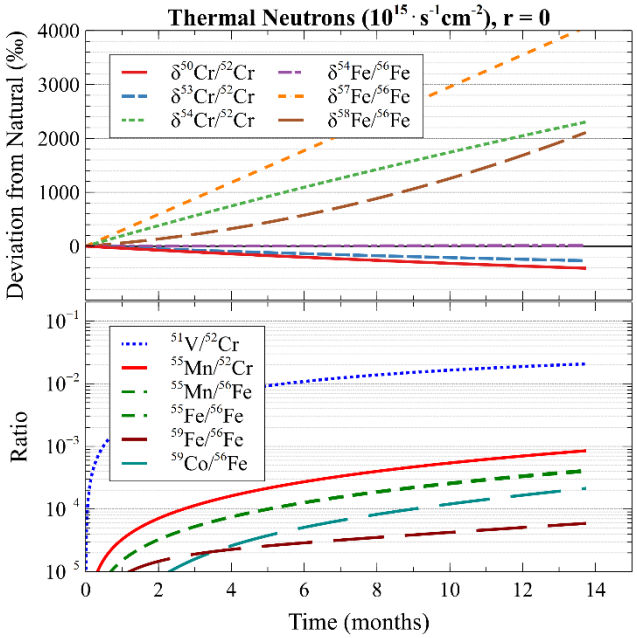

Figure 18: Simulated n-capture effects on Cr & Fe isotopes.

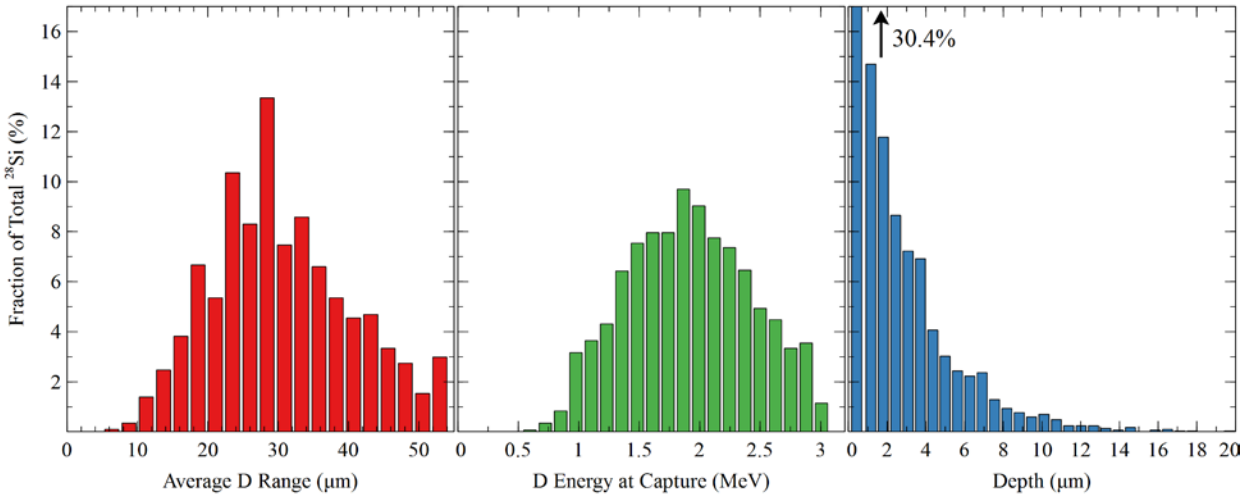

Figure 19: Results from the Monte Carlo ^{27}Al(D,pβ-)^{28}Si simulation. (Left) Distribution of average D ranges for samples drawn from the Hawk energy distribution in Figure 4. (Middle) Distribution of D energies when a ^{27}Al(D,pβ-)^{28}Si reaction occurred. (Right) Simulated depth profile of ^{28}Si.

ACKNOWLEDGEMENTS

We would like to thank several colleagues at NRL for their help facilitating this work. Brian Sobocinski, David Parsons, and Eric Kaiser for their help operating the Hawk pulsed power generator. David Mosher for help estimating the deuteron spectrum from the Hawk DFP. Robert J. Commisso and Paul E. Adamson for helpful discussions regarding the deuteron spectrum.

REFERENCES

1. M. D. DeHart, Z. Karriem, et al., *Progress in Nuclear Energy*, 2018, **104**, 117-135.
2. D. Willingham, B. E. Naes, et al., *Journal of Nuclear Materials*, 2018, **498**, 348-354.
3. E. E. Groopman, D. G. Willingham, et al., *J Anal At Spectrom*, 2020, **35**, 600-625.
4. J. Davis and G. M. Petrov, *Plasma Physics and Controlled Fusion*, 2008, **50**.
5. E. E. Groopman, D. G. Willingham, et al., *Proc Natl Acad Sci U S A*, 2018, **115**, 8676-8681.
6. A. J. Fahey, E. E. Groopman, et al., *Anal Chem*, 2016, **88**, 7145-7153.
7. D. Willingham, E. Groopman, et al., *J Am Soc Mass Spectrom*, 2020, **31**, 1647–1655.
8. D. Willingham, E. E. Groopman, et al., *Analyst*, 2018, **143**, 5364-5371.
9. A. J. Fahey, *Review of Scientific Instruments*, 1998, **69**, 1282-1288.
10. J. W. Mather, *Physics of Fluids*, 1965, **8**.
11. D. E. Potter, *Physics of Fluids*, 1971, **14**.
12. D. Klir, A. V. Shishlov, et al., *Plasma Physics and Controlled Fusion*, 2015, **57**.
13. C. H. Westcott, W. H. Walker, et al., *Effective cross sections and cadmium ratios for the neutron spectra of thermal reactors*, Atomic Energy of Canada Limited, Chalk River, Ont., 1958.
14. K. Shibata, O. Iwamoto, et al., *Journal of Nuclear Science and Technology*, 2011, **48**, 1-30.
15. J. F. Ziegler, M. D. Ziegler, et al., *Nuclear Instruments and Methods in Physics Research Section B: Beam Interactions with Materials and Atoms*, 2010, **268**, 1818-1823.
16. P. M. L. Hedberg, P. Peres, et al., *Journal of Analytical Atomic Spectrometry*, 2015, **30**, 2516-2524.
17. M. R. Kilburn and D. Wacey, in *Principles and Practice of Analytical Techniques in Geosciences*, The Royal Society of Chemistry, 2015, DOI: 10.1039/9781782625025-00001, pp. 1-34.
18. H. R. Peters and J. L. Harlow, eds. E. R. Bradley and G. P. Sabol, ASTM International, West Conshohocken, PA, 1996, DOI: 10.1520/STP16178S, pp. 295-318.